Supplementary Information

Insight into the relationship of redox ability and separation efficiency via the case of α-Bi_2O_3/$Bi_5NO_3O_7$

Jie-hao Li[a,b,#], Rui-hong Liu[a,c,#], Meng Ning[a,c], Yi-lei Li[a,c], Ying Liu[a,c], Xinying Liu[d*], Phathutshedzo Khangale[b], Diane Hildebrandt[e], Xiao-jing Wang[a,c], Fa-tang Li[a,c*]

[a] International Joint Laboratory of New Energy, Hebei University of Science and Technology, Shijiazhuang 050018, China

[b] Department of Chemical Engineering, University of Johannesburg, Johannesburg 2028, South Africa

[c] Hebei Key Laboratory of Photoelectric Control on Surface and Interface, College of Science, Hebei University of Science and Technology, Shijiazhuang 050018, China.

[d] Institute for the Development of Energy for African Sustainability (IDEAS), University of South Africa (UNISA), Florida 1710, South Africa.

[e] African Energy Leadership Centre, WITS Business School & Molecular Science Institute, School of Chemistry, University of Witwatersrand, Johannesburg, 2050, South Africa

Experimental

Characterization of catalysts

Photoelectrochemical measurements were measured on an electrochemical workstation (Chenhua CHI-660E). The instrument contains a three-electrode quartz cell, with a platinum electrode as the counter electrode, an Ag/AgCl electrode as the reference electrode, and a conductive glass plate (ITO) coated with the samples as the working electrode. The electrolyte was a 0.2 mol/L Na_2SO_4 aqueous solution, and simulated visible-light and ultraviolet light were provided by a 300 W Xe lamp (UV filter or λ>400nm filter).

Table S1. The fitted lifetimes and the corresponding percentage of BNO, 0.744BBNO and α-Bi_2O_3

Sample	**τ_1(ns)**	**P_1(%)**	**τ_2(ns)**	**P_2(%)**	**τ_3(ns)**	**P_3(%)**	**τ_{ave}**
BNO	0.0767	52.37	1.9168	31.78	9.0695	15.85	6.81
0.744BBNO	0.1814	44.43	2.2732	36.09	11.5537	19.47	8.85
α-Bi_2O_3	0.0391	39.93	1.8974	40.61	9.2643	19.46	7.02

Table S2. The Zeta potential of BNO, 0.744BBNO and α-Bi_2O_3

Sample	Zeta potential (mV)
BNO	-40.3
0.744BBNO	-23.6
α-Bi_2O_3	-19.3

Table S3. A comparison of the scientific value of the current work with the existing literature.

Sample	Pollutant concentration	Degradation activity	Reason	Reference
2%Mo-BiOBr	10 mg/L sulfanilamide solution	2%Mo-BiOBr is 4.7 times higher than pure BiOBr	Doping improves separation efficiency	1
BCN-200/rGO	10 mg/L CIP	BCN-200/rGO is 9.0 times higher than pure Bi_2WO_6, 2.1 times of pure g-C_3N_4	Improved separation efficiency	2
Bi_2MoO_6/Ti_3C_2	TC	Bi_2MoO_6/Ti_3C_2 is 8.8 times higher than pure Bi_2MoO_6, 1.3 times of pure Ti_3C_2	Heterojunction improves separation efficiency	3
β-$Bi_2O_3/Bi_2O_2CO_3$	10 mg/L RhB	Heterojunction is high activity in Vis-light, but pure $Bi_2O_2CO_3$ is high activity under UV-light.	The upward shift of the valence band of $Bi_2O_2CO_3$ reduces the oxidation capacity, but improves the separation efficiency	4

$Bi_3O_4Br/\alpha\text{-}Bi_2O_3$	10 mg/L MO, 50 mg/L Phenol	$Bi_3O_4Br/\alpha\text{-}Bi_2O_3$ is 11.6 times higher than pure Bi_3O_4Br, 5.2 times of pure α-Bi_2O_3 under MO; $Bi_3O_4Br/\alpha\text{-}Bi_2O_3$ is 1.4 times higher than pure Bi_3O_4Br, 3.3 times of pure α-Bi_2O_3 under phenol	The downward movement of the Bi_2O_3 VB position improves its oxidation capacity, but reduces the separation efficiency of the photogenerated carriers	5
$FeV_2O_4\text{-}Bi_2O_3$	25 mg/L MB	$FeV_2O_4\text{-}Bi_2O_3$ is 7 times higher than pure FeV_2O_4, 4.6 times of pure Bi_2O_3	FeV_2O_4 decorated Bi_2O_3 improves separation efficiency	6
0.744BBNO	10 mg/L RhB, 20 mg/L TC	Heterojunction activity is lower than pure substances	Heterojunction formation reduces the ability to generate reactive species	Present study

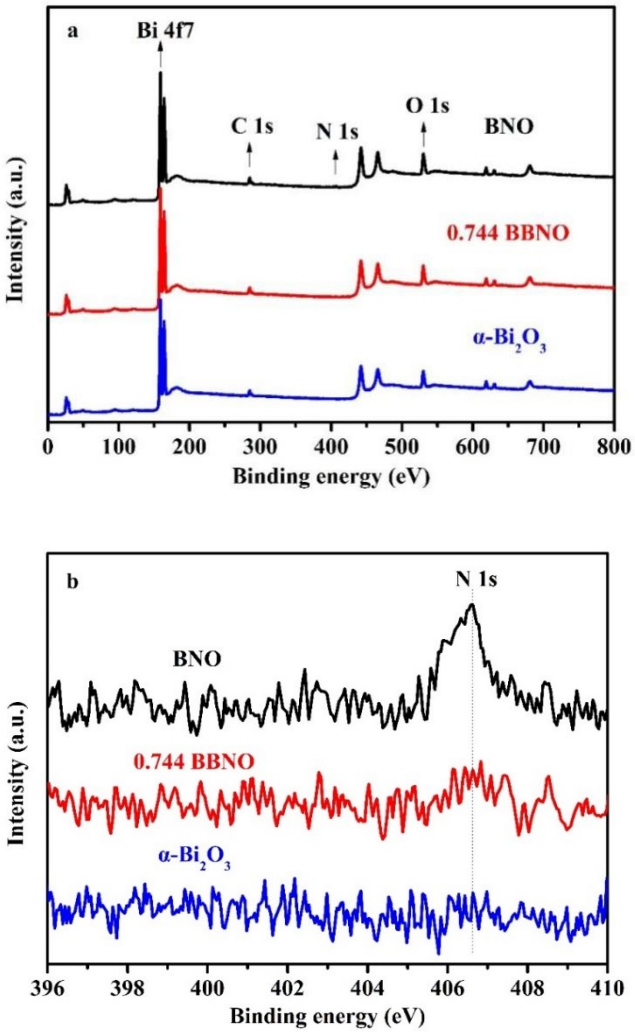

Fig. S1. a) XPS spectra and b) N 1s high resolution XPS spectra over BNO, 0.744BBNO and α-Bi_2O_3 samples.

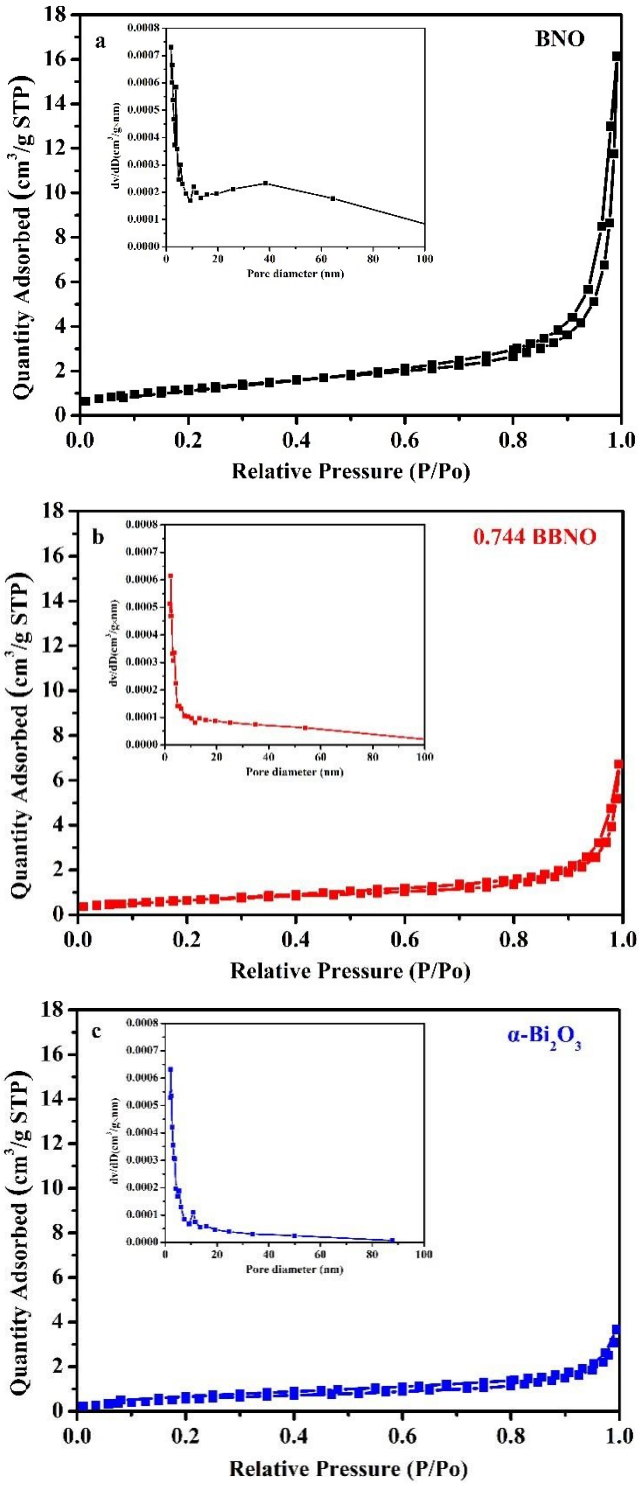

Fig. S2. a), b) and c): Nitrogen adsorption-desorption isotherms and pore size distributions of the BNO, 0.744BBNO and α-Bi_2O_3 samples.

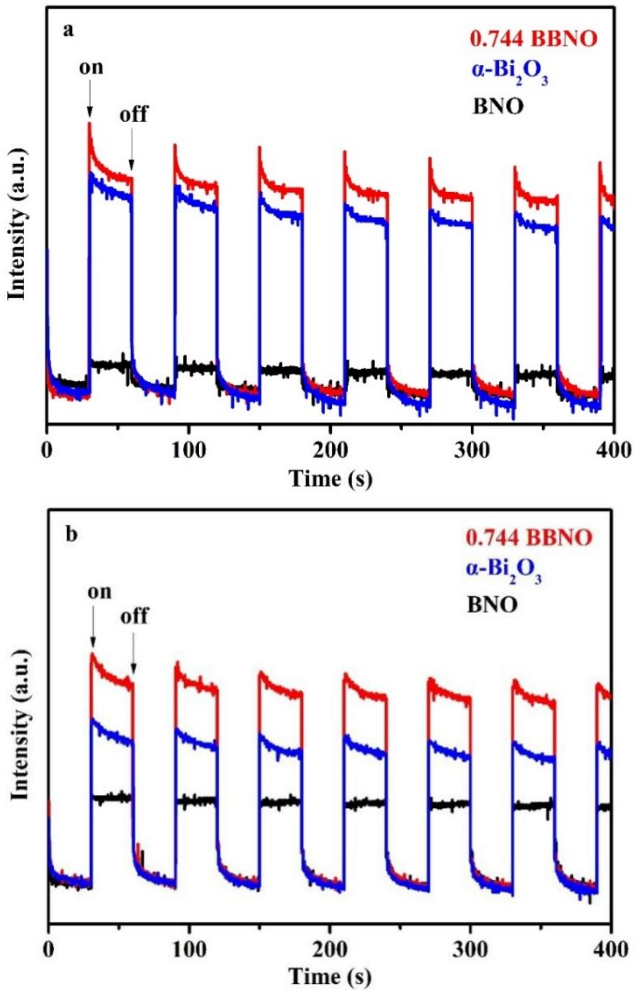

Fig. S3. a) Visible-light and b) UV-light transient photocurrent plots of the BNO, 0.744BBNO and α-Bi_2O_3 samples.

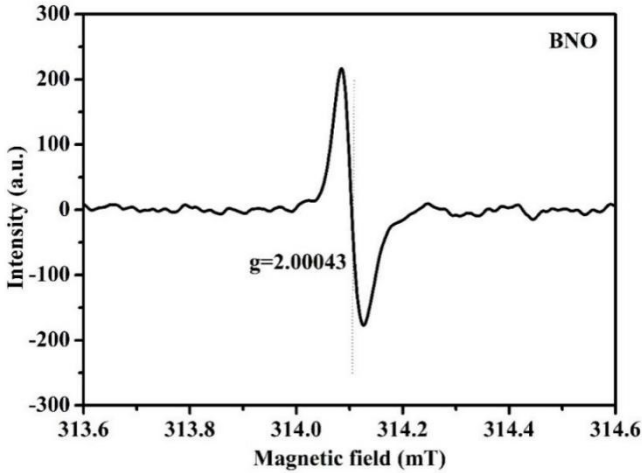

Fig. S4. Solid state EPR patterns of BNO.

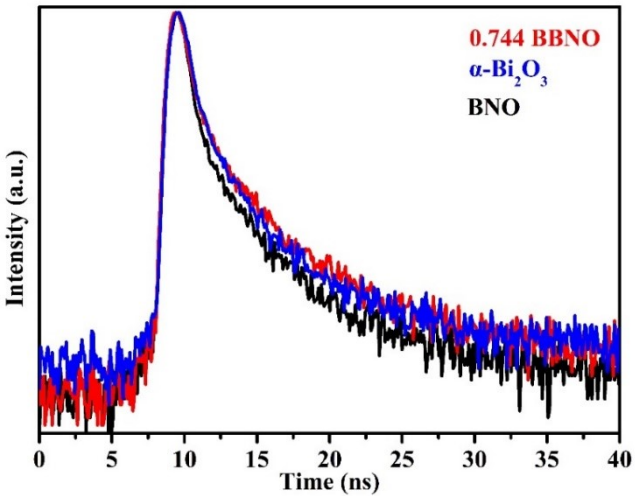

Fig. S5. Transient fluorescence of the BNO, 0.744BBNO and α-Bi_2O_3 samples.

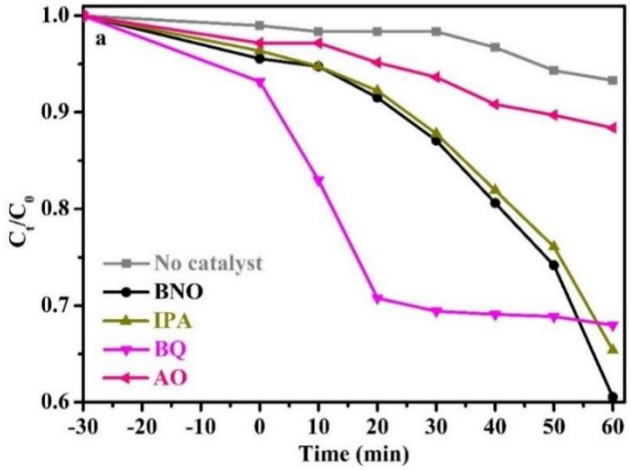
a
No catalyst
BNO
IPA
BQ
AO
C_t/C_0
Time (min)

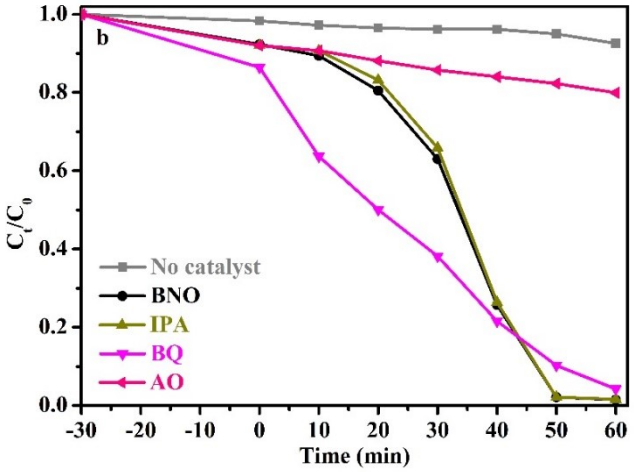
b
No catalyst
BNO
IPA
BQ
AO
C_t/C_0
Time (min)

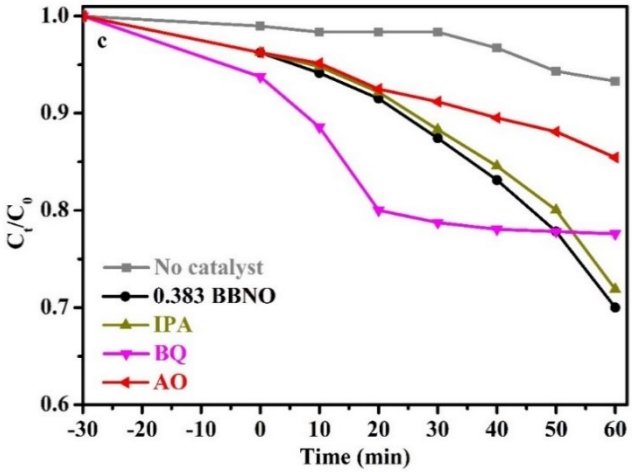
c
No catalyst
0.383 BBNO
IPA
BQ
AO
C_t/C_0
Time (min)

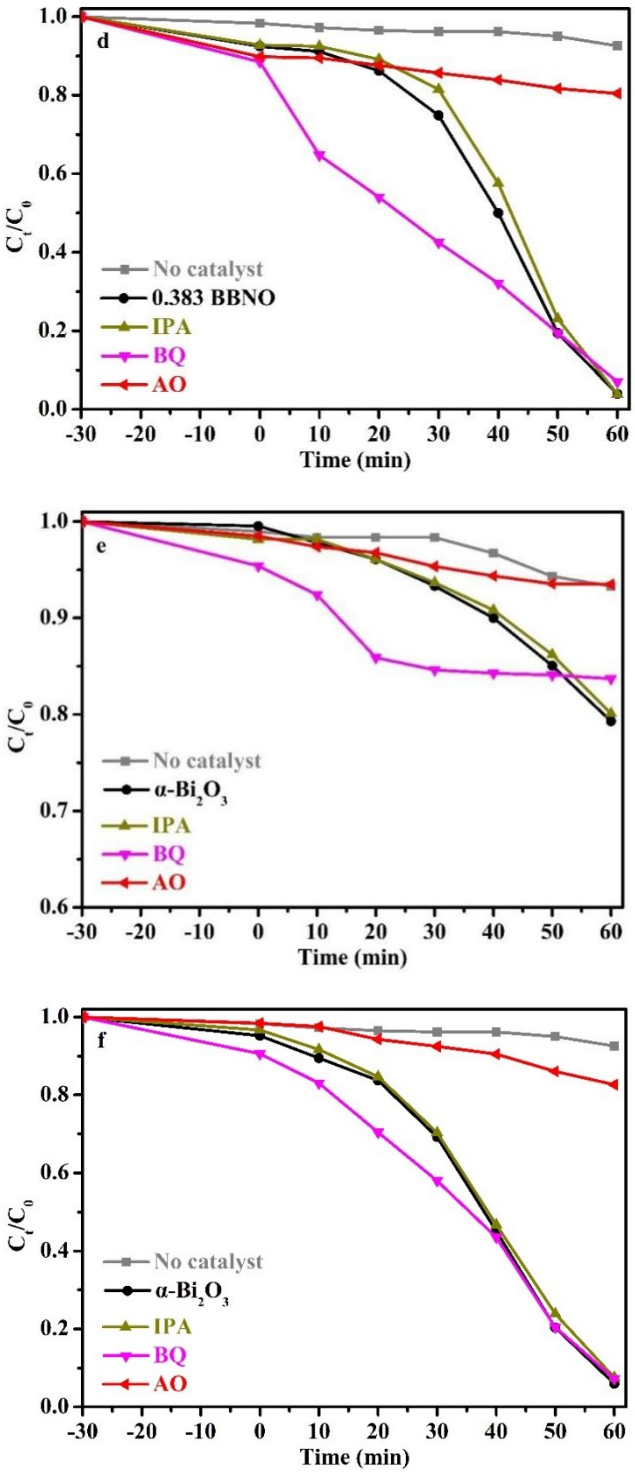

Fig. S6. a), c) and e): Scavenger experiments (RhB) of BNO, 0.383BBNO and α-Bi_2O_3 under Vis-light. b), d) and f):Scavenger experiments (RhB) of BNO, 0.383BBNO and α-Bi_2O_3 under UV-light.

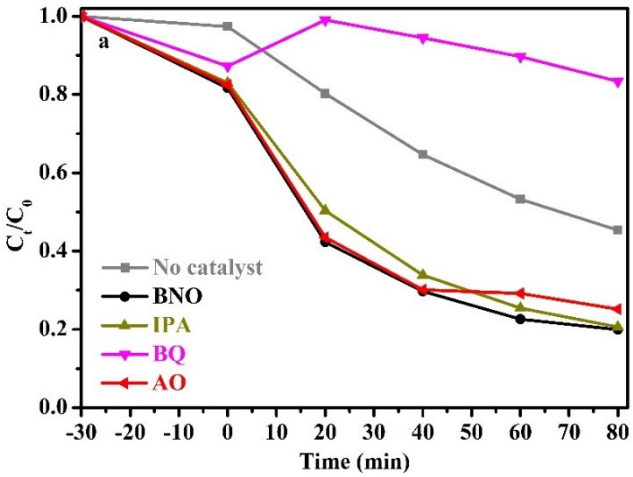
a
No catalyst
BNO
IPA
BQ
AO
C_t/C_0
Time (min)

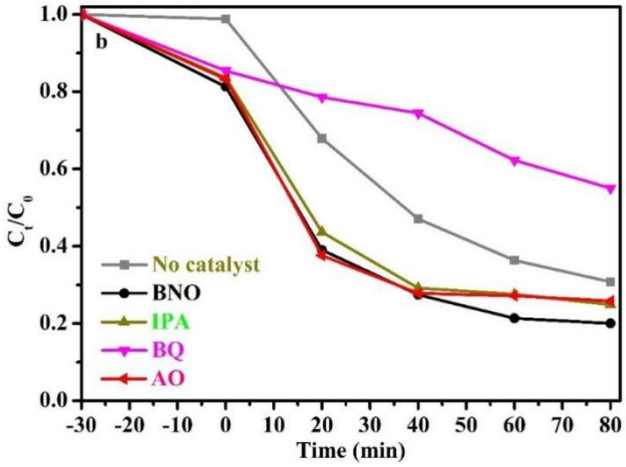
b
No catalyst
BNO
IPA
BQ
AO
C_t/C_0
Time (min)

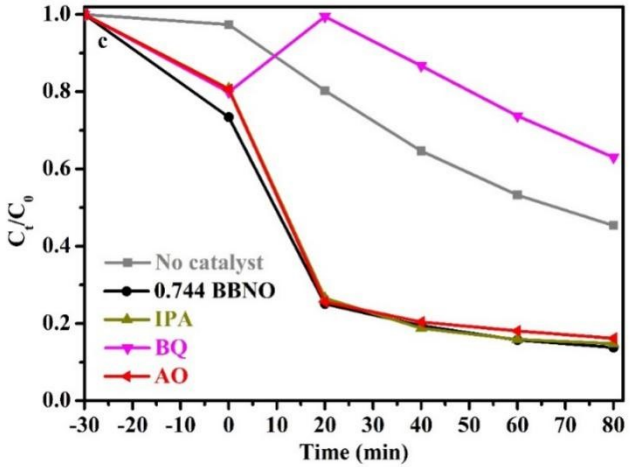
c
No catalyst
0.744 BBNO
IPA
BQ
AO
C_t/C_0
Time (min)

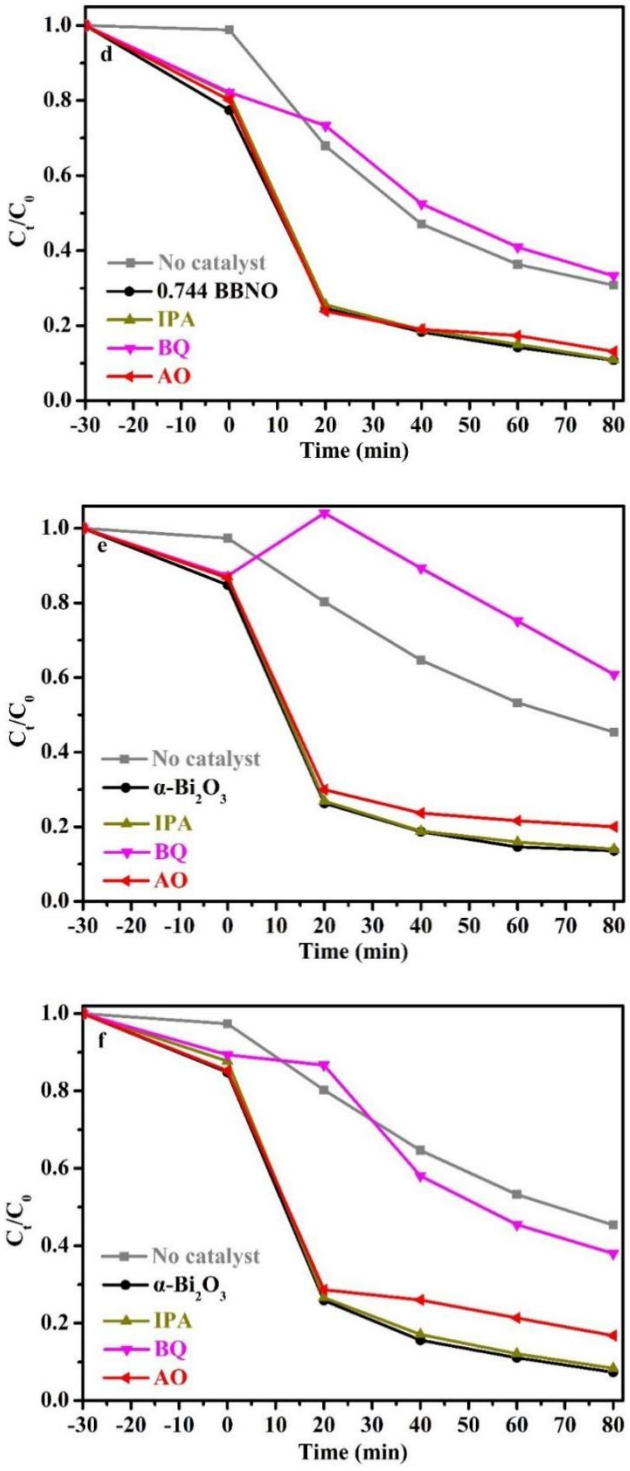

Fig. S7. a), c) and e): Scavenger experiments (TC) of BNO, 0.744BBNO and α-Bi_2O_3 under Vis-light. b), d) and f): Scavenger experiments (TC) of BNO, 0.744BBNO and α-Bi_2O_3 under UV-light.

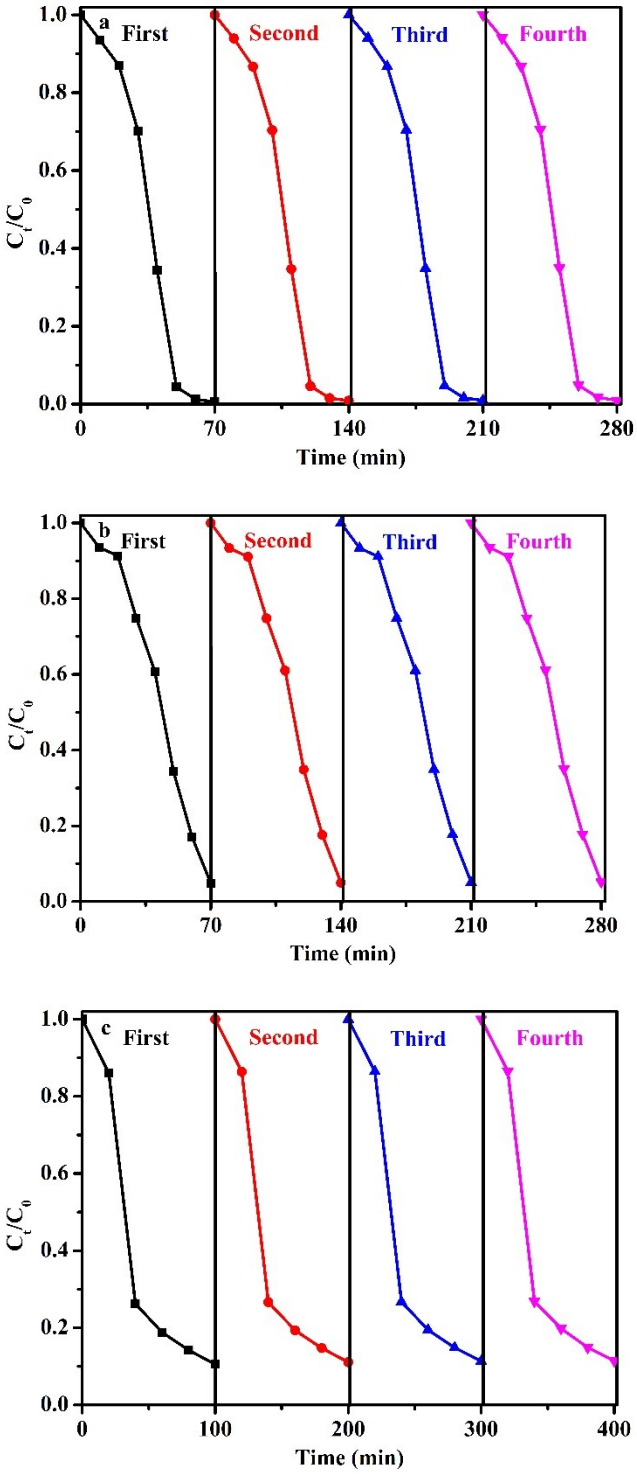

Fig. S8. a), b) and c): Cycles test (RhB) of BNO and 0.744BBNO under UV-light. c): Cycles test (TC) of α-Bi_2O_3 under UV-light.

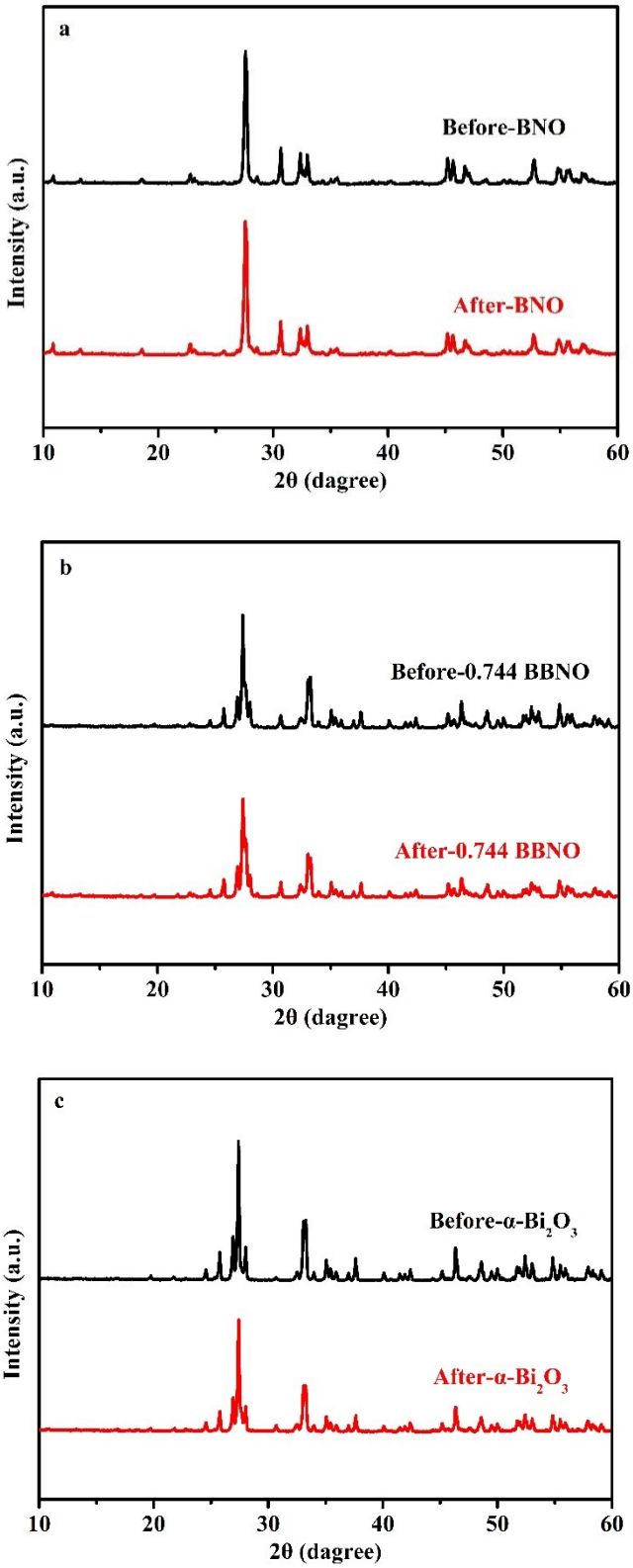

Fig. S9. a), b) and c): XRD spectra of reused BNO, 0.744BBNO and α-Bi_2O_3.

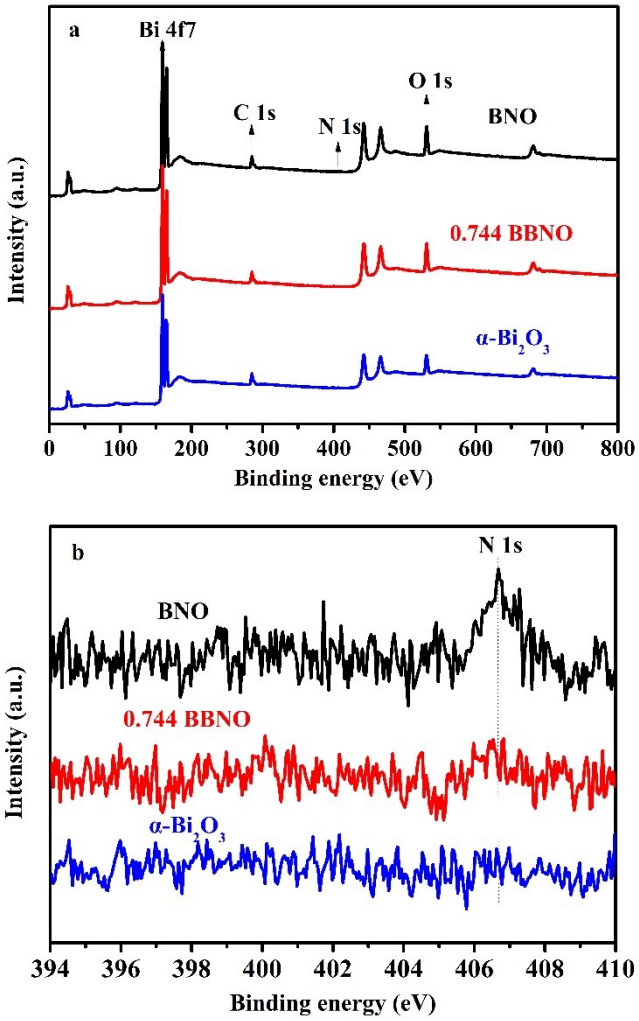

Fig. S10. a) XPS spectra and b) N 1s high resolution XPS spectra over reused BNO, 0.744BBNO and α-Bi_2O_3 samples.

References

1. Y. Y. Wu, H. D. Ji, Q. M. Liu, Z. Y. Sun, P.S. Li, P. R. Ding, M. Guo, X. H. Yi, W. L. Xu, C. C. Wang, S. Gao, Q. Wang, W. Liu and S. W. Chen, Visible Light Photocatalytic Degradation of Sulfanilamide Enhanced by Mo Doping of BiOBr Nanoflowers, *J. Hazard. Mater.,* 2022, **424**, 127563.

2. A. Verma, S. Kumar and Y. P. Fu, A Ternary-hybrid as Efficiently Photocatalytic Antibiotic Degradation and Electrochemical Pollutant Detection, *Chem. Eng. J.,* 2021, **408**, 127290.

3. D. X. Zhao and C. Cai, Preparation of Bi_2MoO_6/Ti_3C_2 MXene heterojunction photocatalysts for fast tetracycline degradation and Cr(VI) reduction,
Inorg. Chem. Front., 2020, **7**, 2799-2808.

4. J. H. Li, J. Ren, Y. J. Hao, E. P. Zhou, Y. Wang, X. J. Wang, R. Su, Y. Liu, X. H. Qi and F. T. Li, Construction of β-$Bi_2O_3/Bi_2O_2CO_3$ Heterojunction Photocatalyst for Deep Understanding the Importance of Separation Efficiency and Valence Band Position, *J. Hazard. Mater.,* 2021, **401**, 123262.

5. J. G. Guo, Y. Liu, Y. J. Hao, Y. L. Li, X. J. Wang, R. H. Liu and F. T. Li, Comparison of Importance Between Separation Efficiency and Valence Band Position: The Case of

Heterostructured $Bi_3O_4Br/\alpha–Bi_2O_3$ Photocatalysts, *Appl Catal B: Environ.,* 2018, **224**, 841–853.
6. B. Janania, S. Swetha, A. Syed, A. M. Elgorban, N. S.S. Zaghloul, Ajith M. Thomas, Lija L. Raju and S. S. Khan, Spinel FeV_2O_4 coupling on nanocube-like Bi_2O_3 for high performance white light photocatalysis and antibacterial applications, J. Alloy. Compd., 2021, **887**, 161432.